SPECTRAL AND OPTICAL PROPERTIES OF OXIDIZED Fe-Mg-Al SMECTITES. V. K. Fox[1], B. Ehlmann[1,2], J. G. Catalano[3], R.J. Kupper[3], R. D. Nickerson[3], S.M. Katz[3], A.A. White[3]; [1] California Institute of Technology (vfox@caltech.edu), [2] Jet Propulsion Laboratory, [3]Washington University in Saint Louis.

Introduction: Secondary minerals produced by aqueous alteration of crustal rocks provide critical clues about the geochemistry, oxidation state, and extent of aqueous activity in the environment in which the secondary minerals formed. Therefore, alteration minerals, particularly phyllosilicates, can be key indicators of the potential habitability of ancient environments throughout the solar system, provided that such minerals can be reliably detected and adequately characterized on other planetary bodies. Due to their ubiquity and geochemical sensitivity to their formation environment [1,2], Fe-, Mg-, and Al-bearing smectites are a key target material in planetary exploration in seeking to understand the aqueous history of the solar system. Despite their importance in planetary science and many studies about Martian clays [e.g., 3–6] and meteorites [7–10], smectite clays have not been comprehensively characterized as standards to allow for accurate and nuanced remote sensing based identification and quantification. Smectite composition can vary nearly continuously between Fe-, Mg-, and Al-rich end members by octahedral cation substitution, along with Al substitution for Si in the tetrahedral layer to balance charge [1,11,12]. The composition and iron oxidation state can be indicative of the conditions in which the clay minerals formed [1,13]. However, the suite of smectite clays commonly used as standards only represent a handful of end-member type compositions. The ability to determine the conditions in which a smectite mineral formed, including the aqueous geochemistry and redox state, and by proxy the potential for habitability, is limited by the ability to accurately identify and measure smectite composition, mineral assemblages and abundance. Detailed characterization of the full compositional range of smectite minerals using techniques analogous to those employed in planetary exploration will help improve those limits.

This abstract presents initial efforts to more fully characterize the complete compositional and oxidation state range of Fe-, Mg- and Al- smectites, in order to allow better identification and characterization of this mineral class using planetary remote sensing. We are synthesizing a suite of mixed Fe/Mg smectites that represent intermediate cation compositions and ferrous, ferric, and mixed valence iron oxidation state. Here we consider ten fully oxidized compositions (Figure 1) and present the initial efforts to characterize the samples using visible to shortwave infrared and thermal emission spectrometry to produce reference libraries appropriate to those remote sensing techniques, and derive optical constants to allow for quantitative abundance modeling with reflectance spectroscopy techniques.

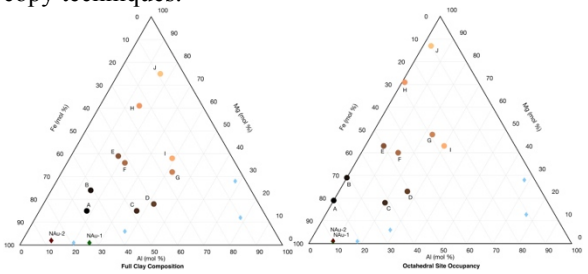

Figure 1: Ternary diagrams showing Fe-Al-Mg content of the ten synthetic smectite samples currently available for analysis. These samples are fully oxidized; increasingly dark color indicates greater iron content. The composition of the full clay structure (octahedral and tetrahedral sheets) is shown on the left. Al substitutes into the tetrahedral layer, such that the composition of the octahedral layer (right), which is the layer used to classify smectites, is relatively depleted in Al. Light blue diamonds are common smectite standards; NAu-1 and NAu-2 are green and red, respectively.

Table 1: Measured mineral formulas of the ten oxidized smectites. Samples are calcium saturated for analysis.

Sample	Measured Formula
A	$Ca_{0.36}Na_{0.09}[Fe^{III}_{1.69}Mg_{0.40}][Si_{3.32}Al_{0.51}Fe^{III}_{0.17}]O_{10}(OH)_2$
B	$Ca_{0.28}[Fe^{III}_{1.54}Mg_{0.64}][Si_{3.55}Al_{0.39}Fe^{III}_{0.06}]O_{10}(OH)_2$
C	$Ca_{0.34}Na_{0.20}[Fe^{III}_{1.24}Mg_{0.37}Al_{0.40}][Si_{3.44}Al_{0.56}]O_{10}(OH)_2$
D	$Ca_{0.35}Na_{0.21}[Fe^{III}_{1.04}Mg_{0.46}Al_{0.54}][Si_{3.45}Al_{0.55}]O_{10}(OH)_2$
E	$Ca_{0.40}[Fe^{III}_{1.06}Mg_{0.93}Al_{0.15}][Si_{3.70}Al_{0.30}]O_{10}(OH)_2$
F	$Ca_{0.32}Na_{0.03}[Fe^{III}_{0.98}Mg_{0.84}Al_{0.30}][Si_{3.80}Al_{0.20}]O_{10}(OH)_2$
G	$Ca_{0.23}[Fe^{III}_{0.69}Mg_{1.12}Al_{0.53}][Si_{3.66}Al_{0.34}]O_{10}(OH)_2$
H	$Ca_{0.39}[Fe^{III}_{0.68}Mg_{1.75}Al_{0.02}][Si_{3.60}Al_{0.40}]O_{10}(OH)_2$
I	$Ca_{0.30}Na_{0.26}[Fe^{III}_{0.57}Mg_{0.92}Al_{0.64}][Si_{3.67}Al_{0.33}]O_{10}(OH)_2$
J	$Ca_{0.37}[Fe^{III}_{0.27}Mg_{2.31}Al_{0.08}][Si_{3.60}Al_{0.40}]O_{10}(OH)_2$

Methods: Smectites were synthesized using a sol-gel procedure [14] with ferric chloride ($FeCl_3 \cdot 6H_2O$) as the iron source. All synthesis steps were performed in air to preserve the fully ferric nature of the clay. Each sample was confirmed to be a single phase using X-ray diffraction. The compositions were determined by lithium metaborate digestion followed by analysis using inductively-coupled plasma optical emission spectroscopy. The spectral reflectances of the 10 samples were collected using an ASD field spectrometer (0.4-2.5 μm) and a Nicolet FTIR spectrometer (1.5-~45 μm). The reflectance spectra shown here are of mixed particle-size powders and aggregates. Optical constants were calculated from measured reflectance spectra of ground and sieved powders.

Initial Results: As expected, infrared spectra show deep vibrational fundamental absorptions at ~2.7-3.0 μm (~3550 cm^{-1}, metal-OH stretch, H_2O stretch) and

6.2 µm (~1660 cm^{-1}, H_2O bending). Si-O stretching modes occur around 1050 cm^{-1} (10 µm) along with M^{3+}-Si-O deformations between 550 and 400 cm^{-1}; samples with greater Mg^{2+} content have a single peak rather than distinct Si-O and M-Si-O features [15] (Fig 2).

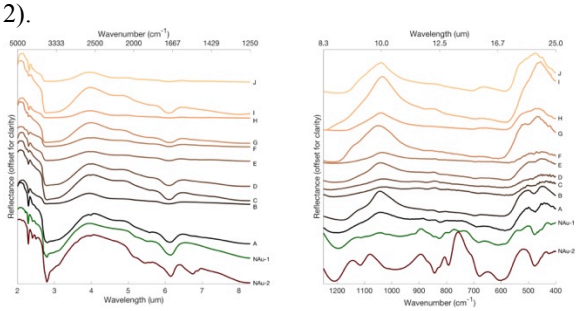

Figure 2. Near to mid-infrared reflectance spectra of the ten ferric samples from 1.5-10 µm (left) and 1250-400 cm^{-1} (right), as well as NAu-1 and NAu-2 for reference. The two plots are scaled to show major features.

Electronic transitions in Fe dominate wavelengths less than 1 µm. Samples with high Fe content have deeper broad absorptions around 0.93 µm and a shoulder around 0.6 µm, and as Fe content decreases narrow absorption near 0.48 µm becomes more defined (Fig 3). Grain size also impacts the relative strength of the bands.

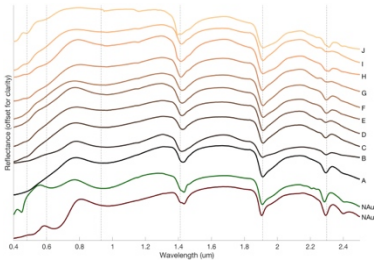

Figure 3. Spectral reflectance from 0.4-2.5 µm of the 10 synthetic samples and Clay Mineral samples. Reference lines shown at 0.48, 0.6, 1.41, 1.9, and 2.3 µm.

In the shortwave infrared, all of the samples have distinct H_2O and OH combination and overtone absorptions at 1.4 µm and 1.9 µm indicating that the clays are hydrated in ambient atmosphere. The wavelength region from ~2.1-2.5 µm exhibits octahedral sheet M-OH vibrational modes for which the wavelength of the absorption minimum shifts, depending on the octahedral sheet cation (Fig 4).

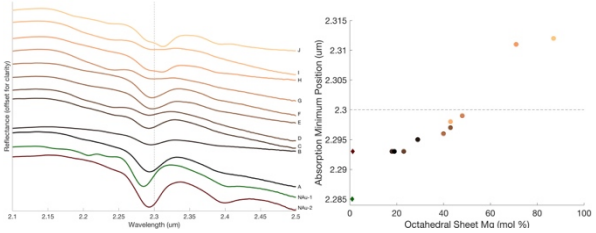

Figure 4: Metal-OH absorptions between 2.1 and 2.5 µm systematically vary with octahedral site composition; darker colors indicate greater iron content.

Mg-rich samples (H and J), which have low iron content, have broader absorptions with reflectance minima longer than 2.31 µm. Higher Fe samples have narrower absorptions centered at less than 2.3µm with a roughly linear relationship with Mg content.

Optical constant derivation and future work: The real and imaginary indices of refraction can be numerically calculated from the measured spectral reflectance. In the visible to near infrared (0.4-2.5 µm), the imaginary index of refraction (k) is calculated using Hapke's scattering model for particulate materials [16–19], assuming an effective particle size and real index of refraction. We pilot test our approach with NAu-1 and NAu-2, which are well-established smectite standards [15,18,20]. Each sample was ground to three particulate sizes (>63 µm >45 µm, >45 µm >25 µm, and >25 µm) and the reflectance properties measured assuming n=1.41. The effective particle size was iteratively adjusted to reduce the residuals of the calculated k values, following [17,18]. Interestingly, the final effective particle size ranged between 5-15 µm for each subsample, likely due to the fact that the true clay particle size is smaller than the aggregate sieved size. In our future work, mid-infrared reflectance spectral measurements will be used to calculate the real and imaginary indices from 5-45 µm using dispersion theory, which will provide an external constraint on the absolute values of n and k [18,20].

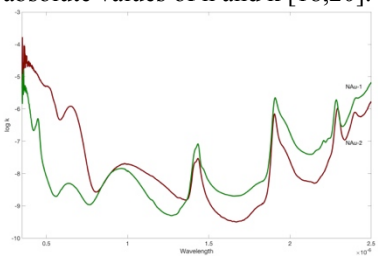

Figure 5: Preliminary derived optical constants for the Fe-rich smectites NAu-1 (green) and NAu-2 (red).

References: [1] Catalano J. G. (2013) *J. Geophys. Res. Planets* **118**, 2124–2136. [2] Ehlmann B. L. et al. (2011) *Nature* **479**, 53–60. [3] Michalski J. R. et al. (2015) *Earth Planet. Sci. Lett.* **427**, 215–225. [4] Bishop J. L. et al. (2008) *Science* **321**, 830–833. [5] Poulet F. et al. (2008) *Astron. Astrophys.* **487**, L41–L44. [6] Bristow T. et al. (2017) p. 2462. [7] Izawa M. R. M. et al. (2010) *Meteorit. Planet. Sci.* **45**, 675–698. [8] Beck P. et al. (2010) *Geochim. Cosmochim. Acta* **74**, 4881–4892. [9] Tomeoka K. and Buseck P. R. (1988) *Geochim. Cosmochim. Acta* **52**, 1627–1640. [10] De Sanctis M. C. et al. (2015) *Nature* **528**, 241–244. [11] Newman A. C. D. (1987) *Chemistry of Clays and Clay Minerals*. [12] Bishop J. L. et al. (2008) *Clay Miner.* **43**, 35–54. [13] Chevrier V. et al. (2007) *Nature* **448**, 60–63. [14] Chemtob S. M. et al. (2015) *J. Geophys. Res. Planets* **120**, 2014JE004763. [15] Michalski J. R. et al. (2005) *Icarus* **174**, 161–177. [16] Hapke B. (2012) *Theory of Reflectance and Emittance Spectroscopy*. [17] Lucey P. G. (1998) *J. Geophys. Res. Planets* **103**, 1703–1713. [18] Roush T. L. (2005) *Icarus* **179**, 259–264. [19] Lapotre M. G. A. et al. (2017) *J. Geophys. Res. Planets* **122**, 983–1009. [20] Glotch T. D. et al. (2007) *Icarus* **192**, 605–622.